SANDIA REPORT

SAND2005-7431
Unlimited Release
Printed December 2005

Probing Deviations from Traditional Colloid Filtration Theory by Atomic Forces Microscopy

Marissa D. Reno

Prepared by
Sandia National Laboratories
Albuquerque, New Mexico 87185 and Livermore, California 94550

Sandia is a multiprogram laboratory operated by Sandia Corporation,
a Lockheed Martin Company, for the United States Department of Energy's
National Nuclear Security Administration under Contract DE-AC04-94AL85000.

Issued by Sandia National Laboratories, operated for the United States Department of Energy by Sandia Corporation.

Available to DOE and DOE contractors from
U.S. Department of Energy
Office of Scientific and Technical Information
P.O. Box 62
Oak Ridge, TN 37831

Telephone: (865) 576-8401
Facsimile: (865) 576-5728
E-Mail: reports@adonis.osti.gov
Online order: http://www.doe.gov/bridge

Available to the public from
U.S. Department of Commerce
National Technical Information Service
5285 Port Royal Rd
Springfield, VA 22161

Telephone: (800) 553-6847
Facsimile: (703) 605-6900
E-Mail: orders@ntis.fedworld.gov
Online order: http://www.ntis.gov/help/ordermethods.asp?loc=7-4-0#online

SAND2005-7431
Unlimited Release
Printed December 2005

Probing Deviations from Traditional Colloid Filtration Theory by Atomic Forces Microscopy

Marissa D. Reno
Sandia National Laboratories
Geohydrology Department
P.O. Box 5800
Albuquerque, New Mexico 87185-0735
mdreno@sandia.gov

Abstract

Colloid transport through saturated media is an integral component of predicting the fate and transport of groundwater contaminants. Developing sound predictive capabilities and establishing effective methodologies for remediation relies heavily on our ability to understand the pertinent physical and chemical mechanisms. Traditionally, colloid transport through saturated media has been described by classical colloid filtration theory (CFT), which predicts an exponential decrease in colloid concentration with travel distance. Furthermore, colloid stability as determined by Derjaguin-Landau-Verwey-Overbeek (DLVO) theory predicts permanent attachment of unstable particles in a primary energy minimum. However, recent studies show significant deviations from these traditional theories. Deposition in the secondary energy minimum has been suggested as a mechanism by which observed deviations can occur. This work investigates the existence of the secondary energy minimum as predicted by DLVO theory using direct force measurements obtained by Atomic Forces Microscopy. Interaction energy as a function of separation distance between a colloid and a quartz surface in electrolyte solutions of varying ionic strength are obtained. Preliminary force measurements show promise and necessary modifications to the current experimental methodology have been identified. Stringent surface cleaning procedures and the use of high-purity water for all injectant solutions is necessary for the most accurate and precise measurements. Comparisons between direct physical measurements by Atomic Forces Microscopy with theoretical calculations and existing experimental findings will allow the evaluation of the existence or absence of a secondary energy minimum.

Acknowledgement

This experimental portion of this work was funded by Sandia National Laboratories' Laboratory Directed Research and Development (LDRD) program. Martin Piech (01816) is thanked for his AFM expertise, which aided in both the general conceptualization of this project and the AFM measurement methodologies.

Table of Contents

List of Figures

List of Tables

1. Introduction

Anthropogenic introduction of contaminants into the subsurface has occurred historically and continues to occur, exacerbating contamination by natural sources, due to intentional land application of fertilizers and pesticides, accidental chemical spills, general waste disposal practices, and geologic isolation of radioactive waste. Developing sound predictive capabilities and establishing effective methodologies for remediation relies heavily on our ability to understand the physical and chemical mechanisms of contaminant transport in the vadose and saturated zones. Colloids, particles with linear dimensions between 1 and 1000 nm, consisting of natural organic and inorganic materials including viruses, bacteria, humic acids, and mineral fragments [*Reimus*, 1995], were identified as a mobile third phase capable of having a significant influence on contaminant transport and mobility in the saturated subsurface [*McCarthy and Zachara*, 1989]. Since then colloids have become an integral component of numerous transport studies in both porous and fractured media. For example, a series of studies have shown that trace metals and radionuclides, which strongly adsorb onto porous media and are generally considered immobile, migrated much further than the distance predicted when the influences of colloids were ignored [*McKay et al.*, 1993; *Kersting et al.*, 1999]. In more general terms, colloids have garnered much attention because they are known to move faster than a conservative dissolved species in groundwater, due to charge and size exclusion, and low diffusivity [*Bales et al.*, 1989; *Grindrod*, 1993; *Reimus*, 1995; *James and Chrysikopoulos*, 2003; *Sirivithayapakorn and Keller*, 2003; *Keller et al.*, 2004].

The transport of colloids through saturated media has traditionally been predicted by accounting for particle advection, hydrodynamic dispersion, and deposition, employing the model of *Yao et al.* [1971], originally introduced as a conceptual model to explain water and wastewater filtration processes. This model is commonly referred to as classical colloid filtration theory (CFT) and, in its simplest form, predicts an exponential decrease in particle concentration with travel distance, where observed concentration varies directly with initial particle concentration and exponentially with particle filtration rate coefficient, travel distance, and interstitial particle velocity. In addition to the predictions based on CFT, with modifications where necessary, it is common in the literature to see additional calculations performed to more clearly elucidate observed concentration breakthrough profiles. These calculations are made using Derjaguin-Landau-Verwey-Overbeek (DLVO) theory, which sums the London-van der Waals attractive interaction, the electrostatic double-layer repulsive interaction, and the Born repulsive interaction to provide the total interaction energy between two surfaces of interest. For some systems (e.g., two surfaces of like charge interacting across an interstitial fluid of relatively high ionic strength), the total interaction energy curve includes both a primary energy minimum, primary energy barrier, and secondary energy minimum, providing two discrete locations (i.e., surface separations) where colloid deposition can occur (see Figure 1) . The secondary energy minimum occurs at a greater separation distance than the primary and, unlike the primary minimum, is not always present. Both CFT and DLVO are given an in-depth treatment in section 2.

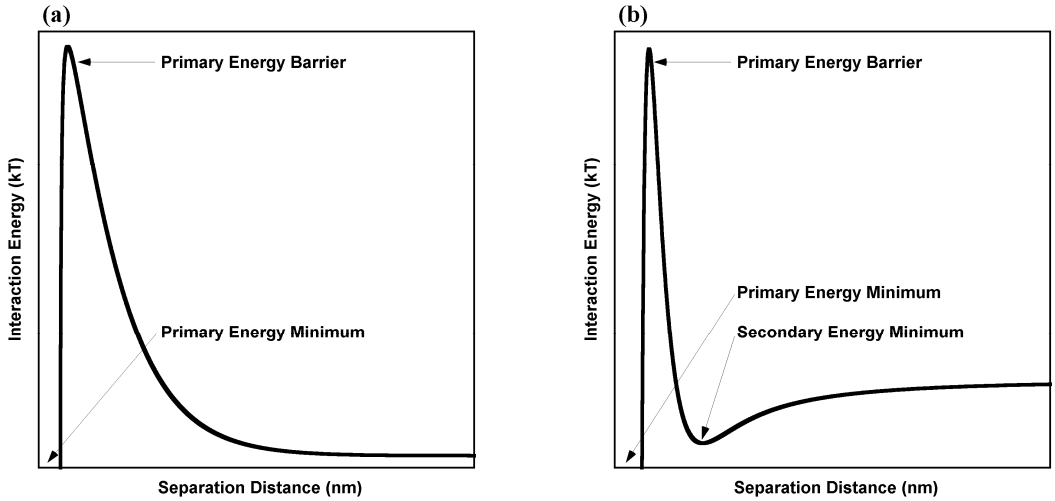

Figure 1: Example interaction energy curves. (a) Primary minimum. (b) Primary and secondary minimum.

Though successful in many cases, the predictive capabilities of colloid filtration and DLVO theories have been heavily scrutinized as the results of numerous porous-media studies that couple experimental breakthrough results with these theoretical predictions show significant deviations. For a packed-bed column of spherical soda-lime glass beads and polystyrene latex colloids, deviations from CFT are evident as ionic strength decreases [*Li et al.*, 2004; *Tufenkji and Elimelech*, 2004b] and become even more pronounced when particle size increases [*Tufenkji and Elimelech*, 2005]. Observations contrary to the predictions of classical CFT have also been observed when surface-charge heterogeneities exist in a system of polystyrene latex spheres interacting with both spherical soda-lime glass beads [*Tufenkji and Elimelech*, 2005] and non-uniform sands [*Roy and Dzombak*, 1996], recombinant Norwalk virus particles interacting with a uniform quartz sand [*Redman et al.*, 2001], and nanolatex particles (95% methyl methacrylate, 5% methacrylic acid) interacting with various mineral substrates [*Antelmi and Spalla*, 1999]. Deviations have also been shown to arise when steric interactions occur [*Tong et al.*, 2005], exclusion [*Bradford et al.*, 2003; *Tufenkji et al.*, 2003] or straining [*Bradford et al.*, 2002; *Bradford et al.*, 2003] mechanisms exist, and for certain experiment length-scales [*Bolster et al.*, 1999].

When deviations arise and are correlated with ionic strength or particle size variations, and/or surface charge heterogeneities, the mechanism which has been suggested to be acting is deposition in the secondary energy minimum, as predicted by DLVO theory. The work by Tufenkji and Elimelech show deviations from CFT arising from both decreases in ionic strength [*Tufenkji and Elimelech*, 2004b] and increases in particle size [*Tufenkji and Elimelech*, 2005]. The latter work shows that deviations associated with ionic strength decreases are less pronounced for smaller particle sizes. These results are consistent with deposition in the secondary energy minimum, which becomes less influential (i.e., its depth decreases) with decreasing particle size. *Hahn et al.* [2004] conducted several deposition and reentrainment experiments, using sulfate-modified latex spherical particles and packed-bed spherical glass bead columns, where solution ionic strength, particle size, and system Hamaker constant were varied. They observed a release of deposited particles following a decrease in ionic strength,

which is not consistent with deposition in a primary minimum, but is consistent with deposition in a secondary minimum. Similarly, *Redman et al.* [2004] show an increase in deposition of bacteria onto quartz grains as solution ionic strength increases and a subsequent release of deposited particles when a solution of lower ionic strength is introduced, phenomena again consistent with deposition in the secondary energy minimum.

Direct measurement of the interaction forces predicted by DLVO theory is possible by the Surface Forces Apparatus (SFA), Total Internal Reflection Microscopy (TIRM), and the Atomic Force Microscope (AFM) [*Israelachvili*, 1992]. It is therefore not unreasonable to assume it possible to directly detect the secondary energy minimum as predicted by DLVO theory. Direct measurement of the forces between a single colloidal particle and substrate of interest is well documented [*Ducker et al.*, 1992; *Toikka et al.*, 1996; *Bowen et al.*, 1999; *Bowen and Doneva*, 2000; *Bowen et al.*, 2002; *Brant and Childress*, 2002; *Assemi et al.*, 2004]; however, the measurement of the secondary energy minimum is not. The one case where it has been measured is for an induced depletion interaction between silica surfaces when a nonadsorbing polyelectrolyte is introduced [*Biggs et al.*, 2000].

This study seeks to directly investigate the existence of a secondary energy minimum using the AFM and colloid probe technique [*Ducker et al.*, 1991]. As a base case, the system presented in *Tufenkji and Elimelech* [2005] will be examined. This work has the potential to contribute to the advancement of colloid transport research because, as the body of evidence showing deviations from traditional CFT grows, so do the number of works proposing mechanisms to explain these deviations (e.g., straining, exclusion, deposition at grain-grain contacts, deposition in the secondary energy minimum). To date, no single mechanism has unanimous support. Direct observation of the secondary energy minimum in one of the systems for which it is argued would therefore be a valuable addition to this area of science.

2. Theory

2.1. DLVO Theory

The total interaction energy between any two surfaces, including colloidal particles, will determine whether or not the system is unstable (i.e., surfaces are attracted to one another; flocculation occurs) or stable (i.e., surfaces are not attracted to one another; dispersion occurs). In terms of colloid transport, negative total interaction energy indicates the dominance of attractive forces and filtration of colloids can occur. Alternatively, positive total interaction energy indicates the dominance of repulsive forces and we expect relatively uninhibited transport in the absence of physical filtering. The total interaction energy between two surfaces is commonly described by the DLVO theory of colloid stability, named after its developers *Derjaguin and Landau* [1941] and *Verwey and Overbeek* [1948], which quantitatively combines the attractive van der Waals interaction, the repulsive electrostatic double layer interaction, and the repulsive Born interaction.

Attractive van der Waals forces are always present in intermolecular interactions, and therefore are a critical component to consider, even though they may be weak compared to other intermolecular forces such as Coulombic (ionic) or H-bonding interactions. The attractive van der Waals force for a sphere-plate interaction (W_{vdwSP}) can be calculated as follows, after *Israelachvili* [1992]:

$$W_{vdwSP} = -\frac{AR}{6D} \tag{1}$$

where A is the Hamaker constant, R is the sphere radius, and D is the distance separating the sphere and the plate. It is important to note that D ranges from D' to ∞, where D' is the closest approach distance. Of the three parameters on which W_{vdwSP} depends, the Hamaker constant is the most difficult to determine. The conventional form of A, after *Israelachvili* [1992] and *Adamson and Gast* [1997], is denoted

$$A = \pi^2 C \rho_1 \rho_2 \tag{2}$$

where C is a constant that depends on the type of interaction (e.g., atom-atom, sphere-sphere, atom-surface, sphere-surface, etc), and ρ_1 and ρ_2 are the number of atoms per unit volume in the two interacting bodies. For media 1 and 2 interacting across medium 3, *Israelachvili* [1992] reports the Hamaker constant based on Lifshitz theory as

$$A \approx \frac{3}{4} kT \left(\frac{\varepsilon_1 - \varepsilon_3}{\varepsilon_1 + \varepsilon_3} \right) \left(\frac{\varepsilon_2 - \varepsilon_3}{\varepsilon_2 + \varepsilon_3} \right) + \frac{3h}{4\pi} \int_{n=0,1,\ldots}^{\infty} \left(\frac{\varepsilon_1(iv_n) - \varepsilon_3(iv_n)}{\varepsilon_1(iv_n) + \varepsilon_3(iv_n)} \right) \left(\frac{\varepsilon_2(iv_n) - \varepsilon_3(iv_n)}{\varepsilon_2(iv_n) + \varepsilon_3(iv_n)} \right) dv \tag{3}$$

where k is Boltzmann's constant (1.38×10^{-23}J/K), T is absolute temperature, ε_i denotes the real dielectric constant (or relative permittivity) of media i, h is Planck's constant (6.625×10^{-34}J·s), ε(iv) are the values of ε at imaginary frequencies, and $v_n = (2\pi kT/h)n$. The quotient kT represents the thermal energy of a system and is often used to gauge the strength of interaction forces, where a force must be greater than kT to overcome the effects of random thermal motion.

In practice, several researchers investigating sphere-plate interactions [*Hahn and O'Melia*, 2004; *Tufenkji and Elimelech*, 2004b, 2005] use in the place (1) of an expression proposed by [*Gregory*, 1981], which claims to be a more accurate expression for W_{vdwSP} because it includes a term to correct for the fact that the Hamaker constant expression was originally derived for a plate-plate interaction (note that equation 3 is an approximate expression). The corrected equation is given by

$$W_{vdwSP} = \left\{ -\frac{AR}{6D} \right\} \left[1 + \left(\frac{14D}{\lambda} \right) \right]^{-1} \tag{4}$$

where λ is the characteristic wavelength of the dispersion interaction and is often taken to be 100 nm [*Gregory*, 1981].

There are very few cases where van der Waals forces alone determine the interaction between two surfaces. In systems where colloidal particles are concerned, the presence of a fluid phase introduces a tremendous amount of complexity, including the occurrence of long-range electrostatic forces. Surfaces become charged in liquid when surface functional groups dissociate or become ionized (i.e., -COOH ↔ -COO- + H+), or

when ions from solution adsorb onto a previously uncharged surface. Independent of the charging mechanism, the equilibrium surface charge will be balanced by the presence of an equal but oppositely charged region of counterions. Counterions that are bound to the surface comprise the Stern or Helmholtz layer, while those counterions at some close separation from the surface form the diffuse electrical double layer. The repulsive electrostatic contribution to the total interaction energy is determined by the nature of the overlap between the diffuse electrical double layers of the interacting surfaces, requiring characterization of the double layer of each surface independently, followed by determination of the nature of overlap between the two. Characterization of individual double layers is generally done using the modified Gouy-Chapman theory, which describes the ions in the diffuse part of the electrical double layers as point charges distributed according to the Poisson-Boltzmann equation [*Swanton*, 1995]. For a sphere interacting with a planar surface, the repulsive electrostatic contribution to the total interaction energy (W_{RSP}), arising from the overlap of the electrical double layers of the sphere and planar surface respectively, is given by *Hogg et al.* [1965]:

$$W_{RSP} = \pi\varepsilon_0\varepsilon R\left\{2\psi_1\psi_2 \ln\left[\frac{1+\exp(-\kappa D)}{1-\exp(-\kappa D)}\right] + \left(\psi_1^2+\psi_2^2\right)\ln\left[1-\exp(-2\kappa D)\right]\right\} \tag{5}$$

where ε is the dielectric constant (or relative permittivity) of the medium, ε_0 is the permittivity of free space (8.854×10^{-12} $C^2J^{-1}m^{-1}$), ψ_1 and ψ_2 are the surface potentials of the sphere and flat plate, respectively, and κ is the Debye length. The Debye length is, calculated as

$$\kappa = \left(\sum_i \rho_{\infty i} e^2 z_i^2 \Big/ \varepsilon\varepsilon_0 kT\right)^{1/2} \text{ m}^{-1} \tag{6}$$

where subscript *i* denotes the ion of interest, ρ_∞ is the number density of ions in the bulk solution, *e* is the elementary charge (1.602×10^{-19} C), and *z* is the valency of ion *i*. Equation (5) only holds exactly for ψ_1 and/or ψ_2 less than 25 mV and for solution conditions such that the double layer thickness is small compared to the particle size. In practice, zeta-potentials are used in the place of surface potentials, due to the fact that surface potentials are not directly measurable.

The third and final component to the total interaction energy is the repulsive Born interaction energy, valid only at very close separations, accounting for the excluded volume effect at contact [*Swanton*, 1995]. The Born interaction energy is a measure of the free energy associated with the electric field around an ion, i.e., the electrostatic free energy equal to the electrostatic work done in forming the ion, bringing it from zero charge to its full charge [*Israelachvili*, 1992; *Swanton*, 1995]). After *Hahn et al.* [2004], the Born repulsion energy for a sphere-flat plate interaction (W_{BSP}) is calculated as

$$W_{BSP} = \frac{A\sigma_B^6}{7560}\left[\frac{8R+D}{(2R+D)^7} + \frac{6R-D}{D^7}\right] \tag{7}$$

where σ_B is the Born collision diameter, derived experimentally, but generally taken to be 0.5 nm.

The combination of 4, 5, and 7 give the total interaction energy as a function of separation distance for a sphere and a flat plate:

$$W_{totalSP} = W_{vdwSP} + W_{RSP} + W_{BSP} \tag{8}$$

2.2. Extensions of Traditional DLVO Theory

Several modifications have been made to the traditional DLVO theory and a thorough review is given by *Swanton* [1995]. The modifications are of two general types: those that offer additional physical processes not included in classical theory, and those that specifically alter the equations for the attractive van der Waals interaction (4) and the repulsive electrostatic interaction (5).

Additional physical processes that have been identified and taken into consideration are non-spherical particles and non-spherical or non-plate collector surfaces. Calculations using expressions developed for both the attractive van der Waals W_{vdw} and repulsive electrostatic (W_R) interactions that include smooth particles of various geometries (e.g., Lyklema [1991]) have given results suggesting little influence on W_{vdw} [*Czarnecki*, 1986a], while the affect on W_R has not been critically evaluated. Expressions for W_{vdw} and W_R when spherical particles interact in pore-spaces (i.e., cylindrical pore [*Smith III and Deen*, 1980, 1983; *Papadopoulos and Kuo*, 1990] and spherical cavity [*Sengupta and Papadopoulos*, 1992a, b] collectors) have also been developed.

Several modifications to the classical model have been employed in attempts to better match observed data. To account for the repeptisation (i.e., deflocculation) of colloids coagulated in the primary minimum, W_R has been formulated assuming constant charge instead of constant potential, the potential of the outer Hemholtz plane instead of the surface has been used to calculate W_{vdw}, and a distance of closest approach (D') has been defined as equal to twice the distance of the outer Hemholtz plane from the particles surface (0.4 to 1 nm) [*Frens and Overbeek*, 1972; *Frens*, 1978]. In order to interpret anomalous behavior in clay dispersions, researchers have defined $W_{totalSP}$ as $W_{vdwSP} + W_{RSP} + W_{AB}$ where W_{AB} is the force contribution from Lewis acid-base interactions (i.e., electron-acceptor—electron-donor interactions). This modification is typically referred to as the extended-DLVO or XDLVO approach (e.g., [*Meinders et al.*, 1995; *Brant and Childress*, 2002]). Classical DLVO theory has also been altered to account for the effects of ion frictional resistance to colloid coagulation [*van de Ven*, 1988; *Warszynski and van de Ven*, 1990], electrostatic double layer relaxation (i.e., temporally variable potential) [*Dukhin and Lyklema*, 1990], fluctuations in the interaction energy arising from surface roughness and irregular shape or charge of particles [*Adamczyk et al.*, 1985; *Czarnecki*, 1986b], a polydisperse population of particles [*Prieve and Lin*, 1982], a distribution of surface potentials [*Cooper*, 1972], and surface roughness [*van Bree et al.*, 1974]. Electrostatic double layer relaxation gives an additional repulsive force at small separations and can contribute two or three orders of magnitude increase in stability ratio, which is not directly included in the formulation for the total interaction energy, but is an indicator of dispersion or coagulation. The impact of polydisperse population of particles was investigated and found to be too small to be significant. A similar conclusion came of the work investigating a distribution of surface potentials, where the impact was determined negligible for potentials less than 20 mV. On the other hand, surface

roughness has been shown to be an important influence at small separations and corrections to the expressions for W_{vdw} and W_R proposed.

2.3. Traditional Colloid Filtration Theory

For the past 30 years, classical colloid filtration theory (CFT), originally conceptualized by *Yao et al.* [1971], has been used to describe the attachment of colloidal particles to a particle or collector under saturated, steady-state conditions. The development by Yao was for water and waste water filtration processes where a spherical particle was modeled as being capable of being filtered out of the bulk solution by three mechanisms: interception, sedimentation, and diffusion. The temporal and spatial variation of concentration in such a system is described as follows:

$$\frac{\partial C}{\partial t} + \mathbf{v} \cdot \nabla C = D_{bm} \nabla^2 C + \left(1 - \frac{\rho}{\rho_p}\right) \frac{mg}{3\pi\mu d} \frac{\partial C}{\partial z} \tag{9}$$

where C is the local concentration of suspended particles, t is time, $\boldsymbol{v}$ is the local velocity of interstitial fluid, D_{bm} is the diffusion coefficient of suspended particles, ρ and ρ_p are the densities of water and suspended particles respectively, m and d_p are the mass and diameter of the suspended particles, and z is the coordinate in the direction of the gravitational force. This equation cannot be solved analytically, hence numerical techniques or simplifying assumptions must be employed. *Yao et al.* [1971] define a single-collector efficiency (η) as:

$$\eta = \frac{\text{rate at which particles strike collector}}{v_0 C_0 \left(\frac{\pi d_c^2}{4}\right)} \tag{10}$$

where the '0' subscripts indicate properties upstream from the collector and d_c is the collector (i.e., grain) diameter. The single-collector efficiency is then used to describe the spatial component of particle concentration in a packed bed, where steady-state conditions are assumed:

$$\frac{dC}{dL} = -\frac{3}{2} \frac{(1-f)}{d_c} \alpha \eta C \tag{11}$$

where L is bed depth, f is porosity and α is the collision/attachment efficiency factor. Integration of (11) yields a form very similar to that which is commonly referred to as the classical colloid filtration model:

$$\ln \frac{C}{C_o} = -\frac{3}{2}(1-f)\alpha\eta \left(\frac{L}{d_c}\right) \tag{12}$$

where C and C_o are the effluent and influent concentrations for a packed bed.

For steady-state transport through saturated porous media, the concept elucidated in equations (9)–(12) above has been modified to account for the mechanisms governing colloid transport, which are advection, hydrodynamic dispersion, and filtration. The resulting model is the one-dimensional advection–dispersion equation with a first-order

kinetic deposition term and describes the concentration of colloidal particles suspended in the fluid phase, $C(x,t)$ [*Kretzschmar et al.*, 1997; *Grolimund et al.*, 1998], as well as the concentration of retained particles, $S(x,t)$ [*Tufenkji and Elimelech*, 2004b], both as a function of column depth x and time t:

$$\frac{\partial C}{\partial t} = D\frac{\partial^2 C}{\partial x^2} - v\frac{\partial C}{\partial x} - kC \tag{13}$$

$$kC = \frac{\rho_b}{f}\frac{\partial S}{\partial t} \tag{14}$$

where v is the interstitial particle velocity, D is the hydrodynamic dispersion coefficient, ρ_b is the medium bulk density, and k is the particle deposition rate coefficient, commonly related to η via the following equation (as shown in [*Yao et al.*, 1971; *Grolimund et al.*, 1998; *Tufenkji and Elimelech*, 2004a]):

$$k = \frac{3(1-f)}{2d_c}v\alpha\eta \tag{15}$$

For most applications, hydrodynamic dispersion is considered negligible and k is specified as a single value (i.e., it is both spatially and temporally invariant). Equations (13) and (14) can be solved by employing these two simplifications in addition to the assumption of a continuous injection of colloidal particles at initial concentration C_0 and time period t_0 into a column with initial concentration of zero. The resulting solutions are, after *Tufenkji and Elimelech* [2004b]:

$$C(x) = C_0 \exp\left[-\frac{k}{v}x\right] \tag{16}$$

$$S(x) = \frac{t_0 fk}{\rho_b}C(x) = \frac{t_0 fkC_0}{\rho_b}\exp\left[-\frac{k}{v}x\right] \tag{17}$$

Equations (12), (15), (16), and (17) serve as the basis for, or comprise the entirety of, the modeling efforts elucidated in the next section.

2.4. Extensions of Traditional Colloid Filtration Theory

As the complexity of natural systems has come to be better quantified, classical colloid filtration theory as described by equations (12), (15), (16), and (17) has been modified in several attempts to capture various types of complexity, including the implementation of multiple or a distribution of rate constants, addition of terms to account for transport mechanisms other than advection, dispersion, and filtration, including the consideration of surface forces using advanced numerical schemes.

Li et al. [2004] propose a distribution to account for deposition under unfavorable conditions (i.e., particles and collector surfaces of like surface charge), where k takes the form

$$k_i = \exp\left(\gamma_i \sigma_{\ln k} + \mu_{\ln k}\right) \tag{18}$$

where γ_i is a standard, normally distributed random number with mean μ equal to 0 and standard deviation σ equal to 1 for each particle *i*, and μ_{lnk} and σ_{lnk} are the mean and standard deviation of the natural logarithm of the deposition rate coefficient. Also in attempt to account for the occurrence of deposition under unfavorable conditions, and additionally to account for deposition under favorable conditions (i.e., particles and collector surfaces of unlike surface charge), *Tufenkji and Elimelech* [2004b] propose a bimodal distribution of *k*, which is the linear combination of two Gaussian distributions:

$$p(k) = f_{slow} \frac{1}{\sigma_{slow}\sqrt{2\pi}} \exp\left[-\frac{1}{2}\left(\frac{k-\bar{k}_{slow}}{\sigma_{slow}}\right)^2\right] + f_{fast} \frac{1}{\sigma_{fast}\sqrt{2\pi}} \exp\left[-\frac{1}{2}\left(\frac{k-\bar{k}_{fast}}{\sigma_{fast}}\right)^2\right] \tag{19}$$

where $\bar{k}_{slow}$ and $\bar{k}_{fast}$ are the mean deposition rate coefficients, σ_{slow} and σ_{fast} are the standard deviations, and f_{slow} and f_{fast} are the fractions of the total particle population associated with each mode of deposition.

An earlier study by *Tufenkji et al.* [2003] similarly defines distributions $p(k)$ of the deposition rate coefficient; however, the distributions here are normal (20) and log-normal (21), aimed at capturing nonexponential deposition patterns, as predicted by (16) and (17), that arise from charge heterogeneity of microbial particles:

$$p(k)_{normal} = \frac{1}{\sigma\sqrt{2\pi}} \exp\left[-\frac{1}{2}\left(\frac{k-\bar{k}}{\sigma}\right)^2\right] \tag{20}$$

$$p(k)_{\log-normal} = \frac{1}{k\sigma_{\log-normal}\sqrt{2\pi}} \exp\left[-\frac{1}{2}\left(\frac{k-k_{\log-normal}}{\sigma_{\log-normal}}\right)^2\right] \tag{21}$$

where $\bar{k}$ is the mean deposition rate coefficient and σ the standard deviation associated with the normal distribution of *k*, while $k_{\log\text{-normal}}$ and $\sigma_{\log\text{-normal}}$ are the same parameters corresponding to the log-normally distributed *k*. Another effort to capture heterogeneity, by *Redman et al.* [2001], employed and evaluated a power-law distribution of *k* of the from $k(\xi,0) = A\xi^{-a}$ where *A* and exponent *a* are both constants.

The spatial distribution of bacteria in variable length columns is modeled by *Bolster et al.* [1999] using classical CFT where appropriate and a second-order model coupled with dual-deposition rate coefficients where CFT proves inadequate to explain experimental observations. The second-order model, used in the place of (14), implemented by *Bolster et al.* [1999] was originally developed by *Saiers et al.* [1994] and takes the form

$$k\left(\frac{X_{\max}-S}{X_{\max}}\right)C - \frac{\rho_b}{f}k_y S = \frac{\rho_b}{f}\frac{\partial S}{\partial t} \tag{22}$$

where k_y is the entrainment coefficient, X_{max} is the maximum retention capacity of the collector grains, and the quantity involving X_{max} indicates the fraction of collector grains available for deposition. Transport predictions are further improved by including a

dual-alpha model, which involves breaking the bacteria population down into two subpopulations and defining attachment efficiencies for each. This modification manifests itself in a new *S* value for implementation in (14) and is calculated as follows:

$$S_{Total}(x,t) = (F)S_{\alpha high}(x,t) + (1-F)S_{\alpha low}(x,t) \tag{23}$$

where *F* is the fraction of influent bacteria with a high attachment efficiency α_{high}, and $S_{\alpha high}$ and $S_{\alpha low}$ are the concentrations of deposited bacteria with high and low attachment efficiencies respectively.

The traditional CFT model has also been modified by addition of terms while retaining the first-order rate expressions that use a single-value for *k*. *Bradford et al.* [2003] develop a model to account for attachment, straining and exclusion. Arising from Fick's Law, the mass balance for this model is given as

$$\frac{\partial(\theta_w C)}{\partial t} = -\nabla \cdot J_T - E^{att} - E^{str} \tag{24}$$

where θ_w is the volumetric water content, J_T is the sum of advective, dispersive and diffusive colloid fluxes, and E^{att} and E^{str} are the colloid mass transfer terms between the aqueous and soil phases due to colloid attachment and straining, respectively.

Last, the Interaction Force Boundary Layer Model has been proposed [*Speilman and Friedlander*, 1974], which is very similar to the one-dimensional advection-dispersion equation (13) but adds an external $\vec{\mathbf{F}}$ force field

$$\frac{\partial C}{\partial t} + \vec{v}_p \cdot \nabla C = \nabla \cdot \left(\vec{\mathbf{D}} \cdot \nabla C - \frac{\vec{\mathbf{D}} C}{kT} \vec{\mathbf{F}} \right) \tag{25}$$

where $\vec{v}_p$ is the particle velocity vector arising from bulk fluid flow, $\vec{\mathbf{D}}$ is the spatially-dependent particle diffusion coefficient, and $\vec{\mathbf{F}}$ is an external force vector that can be represented as the gradient of the total interaction energy. *Hahn and O'Melia* [2004] demonstrate the use of the Interaction Force Boundary Layer model coupled with Monte Carlo and Brownian Dynamics methods to simulate particle trajectories, replacing (14).

3. Materials and Methods

Direct force measurements between colloidal particles of various diameters and a mineral substrate were performed in KCl solutions of varying ionic strength using atomic forces microscopy. These measurements can provide direct physical evidence for the existence or absence of a secondary energy minimum as predicted by DLVO theory (equation 8).

3.1. Colloidal Particles and Substrate

Surfactant-free fluorescent polystyrene carboxylate-modified microspheres with nominal diameters of 3.2, 2.0 and 1.0 micron (μm) were used as model colloids. The 3.2 μm particles were purchased from Bangs Laboratories (Fishers, IN), product code FC05F/6934. The 2.0 and 1.0 μm particles were purchased from Molecular Probes, now

Invitrogen Corporation (Carlsbad, CA), product codes F8825 and F8819. These particles have a density of 1.055 g/ml and carry a slightly negative surface charge for pH greater than approximately 4 to 5. These particles were chosen based on their size (i.e., they are within the range of natural colloidal particles and big enough to use for the colloid-probe) and ubiquitous use in subsurface transport studies [*Reimus*, 1995], including the study by *Tufenkji and Elimelech* [2005]. Individual colloids were mounted to the ends of tipless silicon nitride probe cantilevers from Veeco Probes (Figure 2). Particle mounting, probe calibration, and spring constant determination were performed by Novascan Technologies.

A polished quartz surface (10-mm diameter, 2-mm thickness) was used as the substrate of interest. The surface was polished to remove any topography that may have compromised the seal between the quartz surface and the fluid cell (discussed below), and also to minimize potential complications arising from micron-scale drift of the colloidal particle once engaged with the surface (i.e., even after the colloid and the surface are engaged, the cantilever-colloid apparatus can drift laterally and if the colloid collides with an obtruding portion of the substrate surface, it may detach from the cantilever). Polishing was performed by Sandia National Laboratories' Processing and Environmental Technology Laboratory. Both surfaces were cleaned prior to making measurements. Ultraviolet (UV) exposure [*Biggs et al.*, 2000], ethanol treatment [*Bowen et al.*, 1999; *Lower et al.*, 2000; *Assemi et al.*, 2004], and thorough rinsing with DI [*Bowen and Doneva*, 2000; *Assemi et al.*, 2004] were used for the quartz surface, while only the ethanol treatment and thorough rinsing with DI was employed for the colloid probes, as it is possible that exposure to an intense UV source could damage the carboxyl surface groups of the colloids.

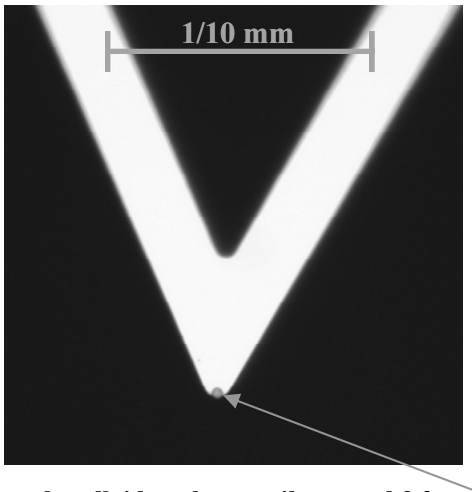

Figure 2: Example colloid probe, cantilever and 3.2 μm colloid only.

3.2. Solution Chemistry

Analytical reagent-grade KCl (Fisher Scientific) and deionized (DI) water were used to prepare all electrolyte solutions. Electrolyte concentrations were prepared such that a range of ionic strengths (10 to 300 mM) could be studied. The pH of all solutions was 6 (non-adjusted pH of DI).

3.3. Electrokinetic Characterization

Electrokinetic characteristics of the individual surfaces (i.e., zeta-potentials, calculated via electrophoretic mobility measurements) and the colloid-electrolyte-quartz system (i.e., the Hamaker constant) as employed in the theoretical calculations that follow are the same as those used for a system of identical colloids and electrolyte solutions, but for soda-lime glass beads [*Tufenkji and Elimelech*, 2004b]. Relevant values are shown in Table 1. For a first approximation, where the relative trends between interaction energies are of primary concern, these values are sufficient; however, it will be advantageous to have direct measurements of the properties of the specific systems employed in this work, and therefore these measurements will be taken at a future date.

A (J)	1×10^{-20}
R (μm)	1.0, 2.0, 3.2
ε_0 ($C^2J^{-1}m^{-1}$)	8.85×10^{-12}
ε	78.5
e (C)	1.60×10^{-19}
k (J/K)	1.38×10^{-23}
T (K)	298.15
z	1
λ (nm)	1×10^{-7}

Table 1: Electrokinetic properties used for DLVO calculations [*Tufenkji and Elimelech*, 2004b].

3.4. AFM Methods

All interaction forces reported on here were measured using a Digital Instruments MultiMode Scanning Probe Microscope with a NanoScope IIIa Controller. A schematic of the instrument is shown in Figure 3. When operated in force mode (a selection made via the NanoScope software), the instrument is referred to as an Atomic Force Microscope (AFM).

With the head of the AFM removed, the sample, in this case the quartz surface mounted with epoxy to a stainless steel disc, is placed on the magnetic sample stage. The colloid probe is placed in the fluid cell (Figure 4) and the fluid cell mounted in the AFM head. The head is then mounted atop the piezoelectric scanner, as shown in the schematic, and the cantilever, sample, and laser aligned. The fluid cell and the sample are then sealed, taking care not to bring the colloid probe into contact with the sample surface. Once all components are properly sealed and aligned, ethanol is introduced into the fluid cell as a final cleaning mechanism. The system is then thoroughly flushed with DI. Electrolyte solutions are then introduced in order of ascending ionic strength (DI, 10 mM, 30 mM, 100 mM, 300 mM). All solutions remained in the flow cell for 30 minutes before the series of force measurements was obtained (see 4.3 Equilibration Time).

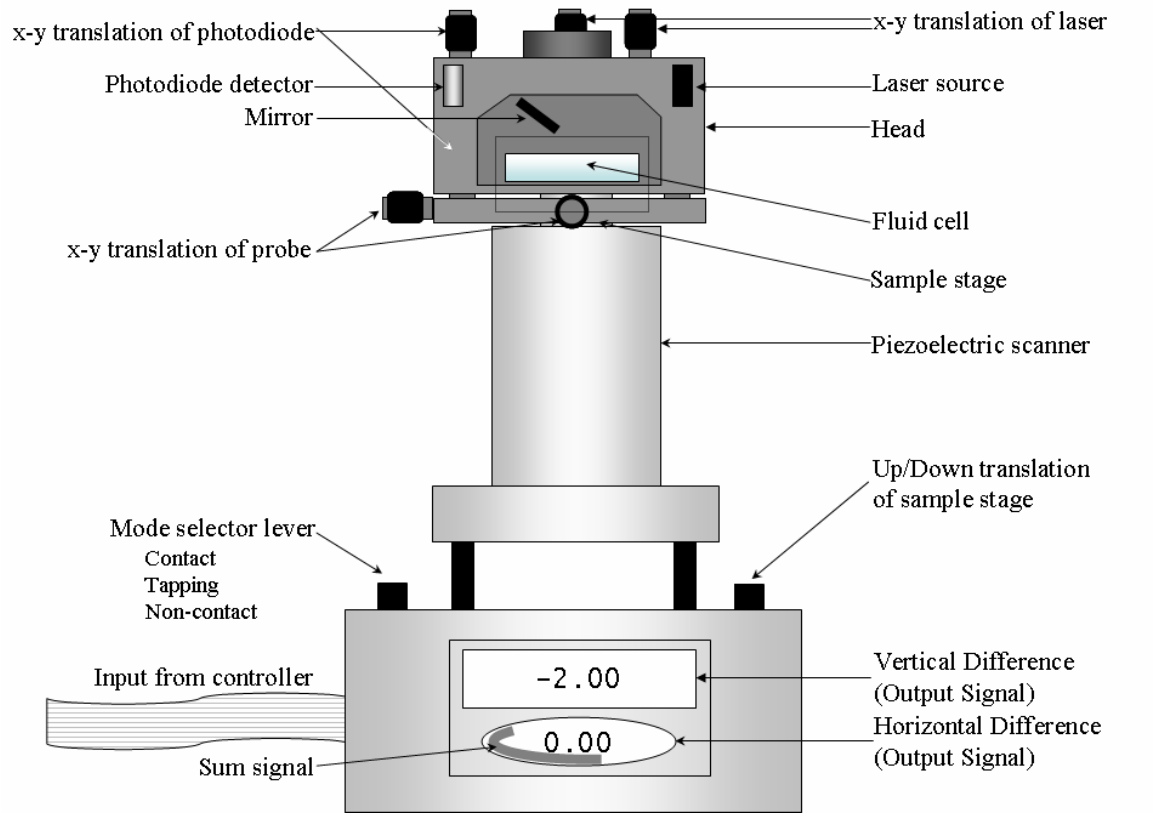

Figure 3: Schematic of the basic components of the Nanoscope MultiMode SPM [*Lord*, 2001].

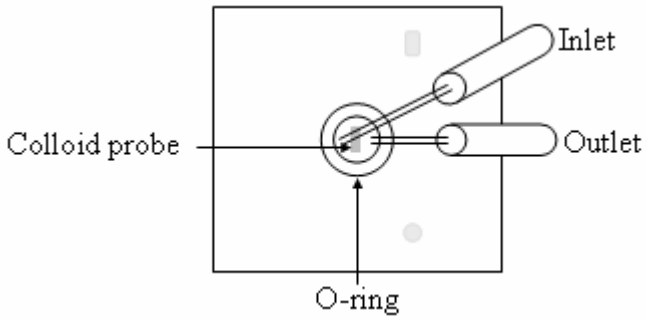

Figure 4: Schematic of fluid cell.

In contact mode, the cantilever (i.e., colloid probe) remains stationary while the sample stage is translated up and down (by the NanoScope IIIa Controller). Deflection of the cantilever results in a change of position of the laser as it enters the photodiode, which is registered and output as voltage (see 'Vertical Difference' in Figure 3). Voltage values (V) were recorded every 1.9 nanometers (nm) with a maximum separation of 3.335 μm. All force measurements were obtained using a scan size of 200 nm and scan rate of 0.250 Hz.

An example of the AFM output (plot only) is shown in Figure 5. The curves show deflection of the cantilever in volts (y-axis) versus piezo displacement in nm (x-axis). Note that two curves result for every sweep: deflection of the cantilever as the surface extends toward the colloid probe and deflection of the cantilever as the surface

retreats from the colloid probe. The 'Extending' curve measures the attractive and repulsive forces between the colloid and the sample, while the 'Retracting' curve measures the adhesive forces between the two. This deflection versus distance data is converted to force versus distance data as follows, where only the extending data is being considered:

1) Define the voltage of zero force (the initial flat, horizontal portion of Figure 5) and subtract this value from all voltage data points.

2) Calculate the slope of the region of constant compliance, that portion of the curve where deflection becomes a linear function of displacement (negatively sloping portion of Figure 5a) and divide all values calculated in 1) by this slope. This gives deflection in nm.

3) Correct the deflection values calculated in 2) as well as the original piezo displacement values by the distance of contact (the slope of the region of constant compliance expressed in nm).

4) Convert deflection values from 3) to force in Newtons (N) by multiplying by the cantilever spring constant (k_s), given in N/m.

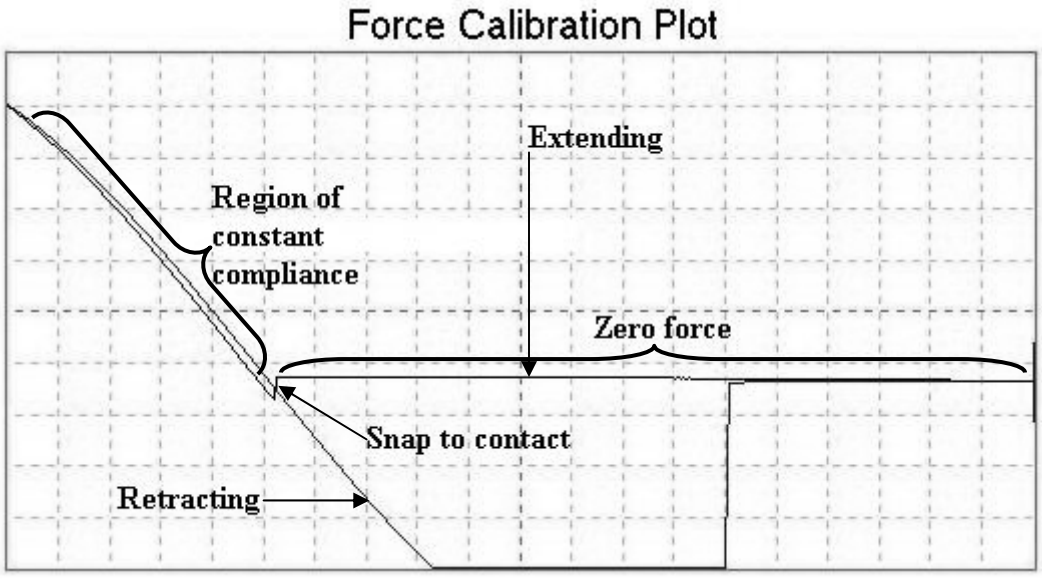

Figure 5: Example AFM output.

4. Results and Discussion

4.1. Theoretical Predictions

Under all experimental conditions employed, it is expected that repulsive forces dominate the interaction between the carboxylate-modified polystyrene spheres (colloids) and quartz. However, as has been suggested, deposition (i.e., attractive interactions) is possible under seemingly unfavorable conditions, and such deposition is attributable to entrapment in a secondary energy minimum. Figure 6 shows the theoretical interaction energy curves (calculated using equation 8) for 1.0, 2.0, and 3.2 μm colloids interacting

with a quartz surface in KCl solutions varying in ionic strength from 10 to 300 mM. For (a) and (b), color designations are shown in the legend and three thicknesses of each color appear. The thickest line is for calculations done assuming the 3.2 μm colloid. The thinner line is for the 2.0 μm colloid, and the dashed line is for the 1.0 μm colloid.

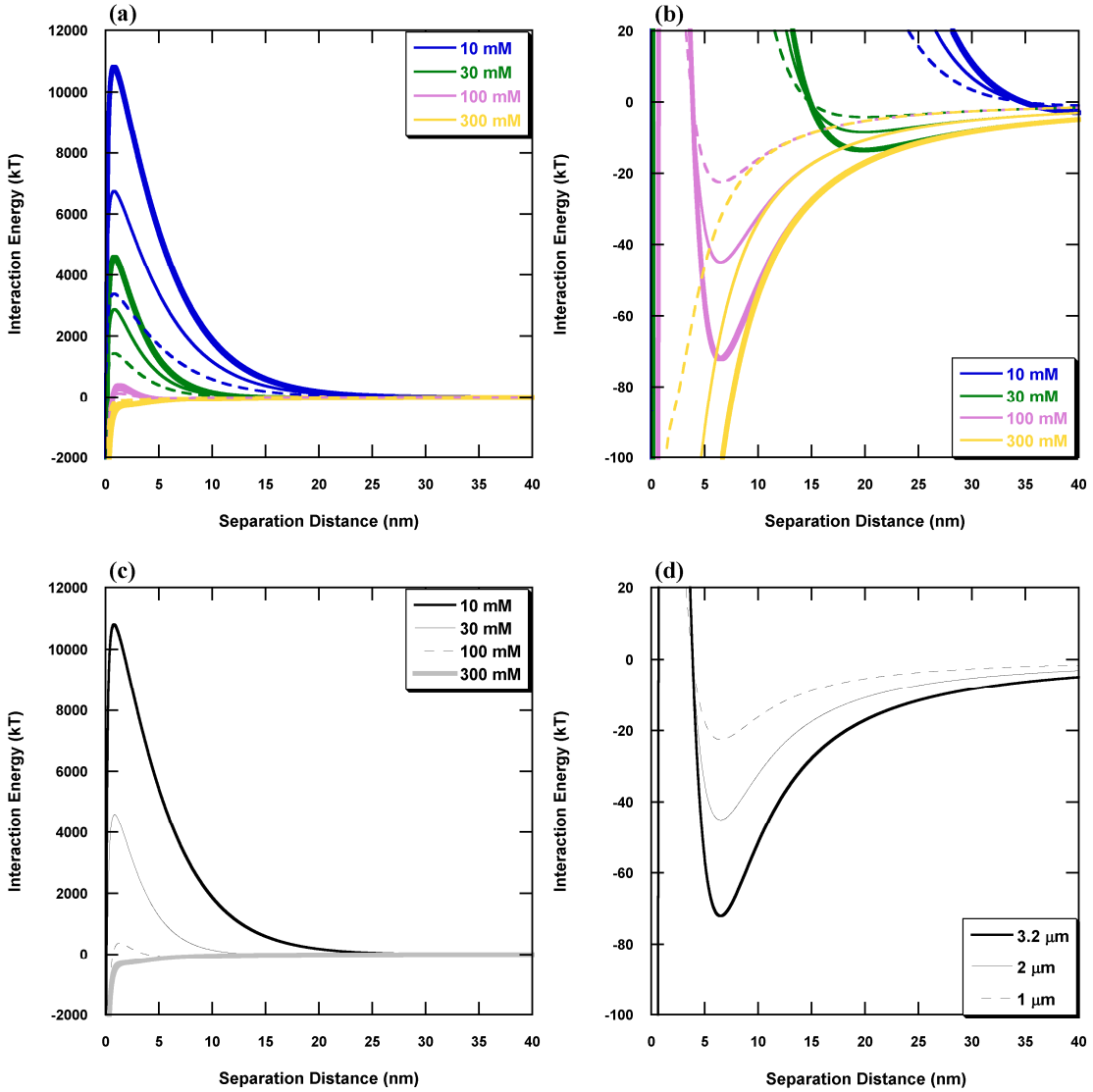

Figure 6: Calculated DLVO interaction energy plotted as a function of separation distance in nm. (a) Interaction energy curves for all particles in KCl solutions of 10, 30, 100 and 300 mM. Line color designates ionic strength; line thickness designates particle size (i.e., thickest = 3.2 μm, thinnest = 2.0 μm, dashed = 1.0 μm). (b) Same as (a), but replotted on a different scale to highlight the location and depth of the secondary minimum. (c) Interaction energy curves for the 3.2 μm colloid in KCl solutions of varying ionic strength, highlighting increasing interaction energy with decreasing ionic strength. (d) Interaction energy curves for all three particles in a 100 mM KCl solution, plotted on a scale similar to (b) to highlight the depth of the secondary minimum.

Figure 6a shows an increasing depth of the secondary energy minimum as ionic strength increases from 10 to 100 mM. For an ionic strength of 300 mM, the interaction is completely attractive. Figure 6b is the same plot as (a), replotted on a scale of smaller range to highlight the location and depth of the secondary minimum. Note that the depth

of the minimum not only increases with ionic strength, but its location gets closer to the surface. Figure 6c highlights the increase in depth of the minimum with increasing ionic strength, while Figure 6d highlights the increase in depth with increase in particle size.

Using the information provided by Figure 6, it is clear that, in order to prove the existence of the secondary energy minimum using direct measurements, it will be necessary to show increasing interaction energy with decreasing ionic strength, as well as increasing interaction energy with decreasing particle size. It is important to note that showing the former alone is a necessary but insufficient indication of a secondary energy minimum. Based on DLVO theory, it is expected that, if it is the primary energy minimum being detected, an increase in interaction energy will be observed as ionic strength decreases (see Figure 6a). Similarly, if it is the secondary energy minimum that is being detected, an increase in interaction energy will also be observed as ionic strength decreases (see Figure 6b). However, as particle size increases, the interaction energy characterizing the primary minimum increases (see Figure 6a), while the interaction energy characterizing the secondary minimum decreases (see Figure 6d). Therefore, it will be necessary to show increasing interaction energy with decreasing ionic strength, as well as decreasing interaction energy with increasing particle size to argue the existence of a secondary energy minimum using direct AFM force measurements.

4.2. General Atomic Force Microscope Data

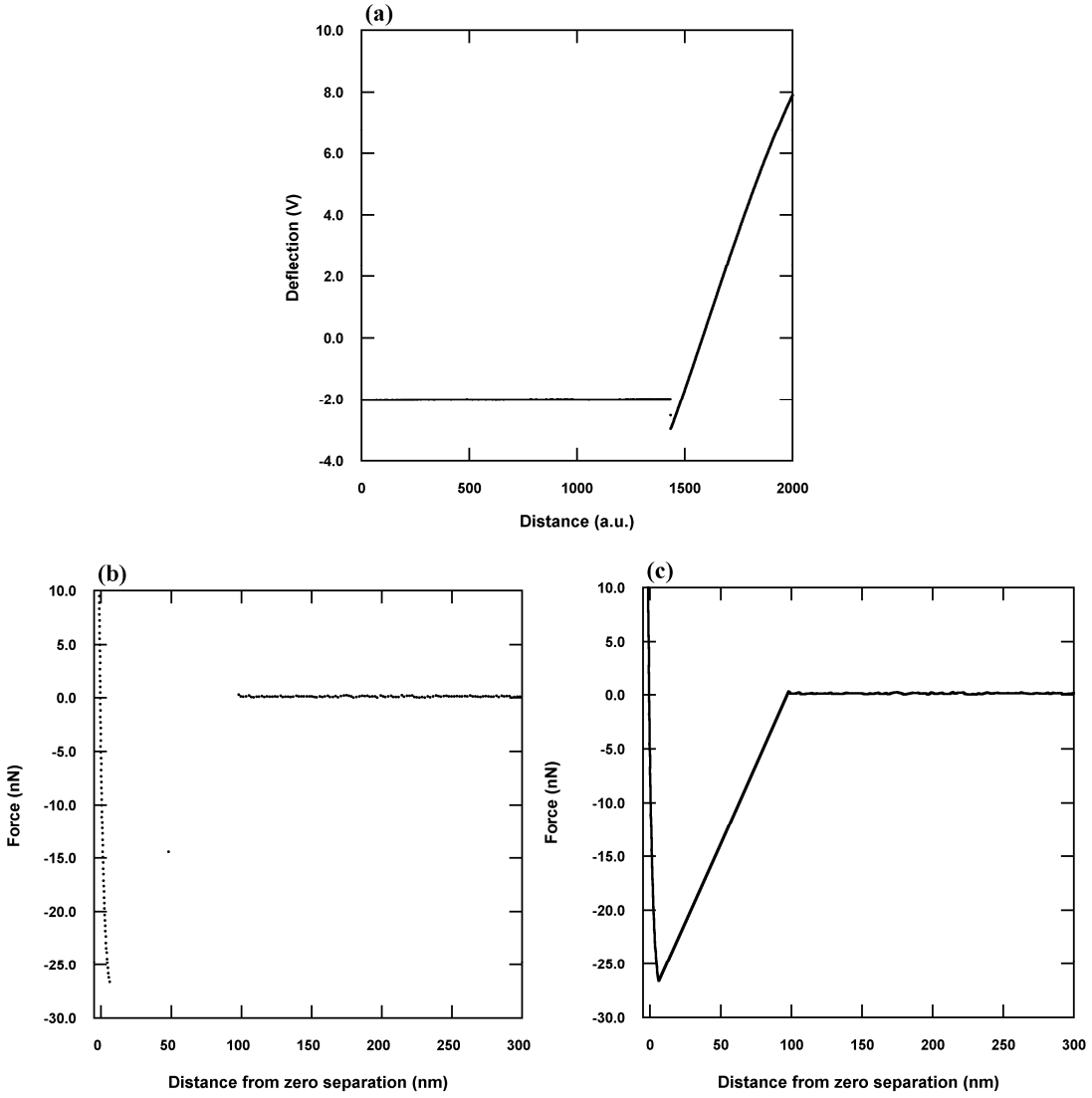

Figure 7: AFM data collected for a 2 μm colloid approaching a polished quartz surface in 100 mM KCl of pH 6. (a) Cantilever deflection versus piezo displacement in arbitrary units, (b) Force (nN) versus distance from zero separation (nm) plotted as discrete data points, and (c) Force (nN) versus distance from zero separation (nm) plotted as a continuous line.

An example of typical AFM output and conversion to useful force data is shown in Figure 7 for a polished quartz surface approaching a 2 μm colloid (k_s = 0.305 N/m) in 100 mM KCl of pH 6. Figure 7a shows deflection of the cantilever in volts versus piezo displacement in nm. Figure 7b gives force in nano-Newtons (nN) versus distance from zero separation in nm, where each discrete data point collected has been converted from the raw deflection output to a force value. Figure 7c shows the same data as Figure 7b, but with the data plotted as a continuous line. It is important to note that only the data collected upon extension (surface approaching cantilever) is shown, as will be the case in all plots that follow. The distinction between Figure 7b and Figure 7c is also important, as Figure 7c makes the assumption that the interaction between 0 nN (separation distance

of approximately 100 nm) and (approximately) -26 nN follows a linear trend. It is hard to say whether or not this assumption is accurate, as only one data point exists between the last point of zero force and the point of contact. For the analyses undertaken here, whether or not the force data truly give a line like that shown in Figure 7c is not important. What is important is the magnitude of force at contact (i.e., the difference in force between the last point of zero force and the first point of contact); however, at this point in this work, only qualitative trends are being examined, hence all force plots shown in this document are shown as Figure 7c is, for ease and elucidation of comparisons made.

4.3. Equilibration Time

A critical component of any experimental study is reproducibility of measurements and subsequent results. As such, demonstrating reproducibility in force measurements is initially the most important aspect of this work. Figure 8 shows raw deflection in volts versus the piezo displacement (Z) distance in nanometers for measurements taken after 0 (a), 20 (b), 30 (c), and 40 (d) minutes of equilibration. Each plot shows the first ten subsequent force curves collected, while Figure 8b-d show the fiftieth force curve (FC_{50}) as well.

For force curves collected after no equilibration (a), drift is observed as the surface approaches the particle ("zero force" portion of curve, refer to Figure 5) and on contact ("constant compliance" portion of curve). The drift observed in the region of constant compliance is highly undesirable, recalling that it is the slope of this region that determines the separation distance of zero needed for generation of all force versus distance curves. As equilibration time is increased from 0 to 20 minutes, a notable improvement is seen in repeatability of measurements in the constant compliance region. Note however, that although improvement is observed in the constant compliance region, significant total drift is observed over the measurement period, as shown by the location of the FC_{50}. Increasing equilibration time from 20 to 30 minutes yields a notable improvement in the entire force curve, where a strong deviation is not observed at later times (i.e., for FC_{50}). The last increase in equilibration time from 30 to 40 minutes shows a similar trend in the region of constant compliance; however, a notable and undesirable drift in the entire force curve is observed at later times. These results suggest that an equilibration time of 30 minutes is optimal, where times both lower and higher yield undesirable drift in the region of constant compliance. For the system being examined here, it is likely that the equilibration time is allowing for the temperature of the introduced fluid and the temperature of the surface to come to equilibrium. These results are supported by the work of *Biggs et al.* [2000], who report allowing 30 minutes for their system to reach stability before force curves were obtained.

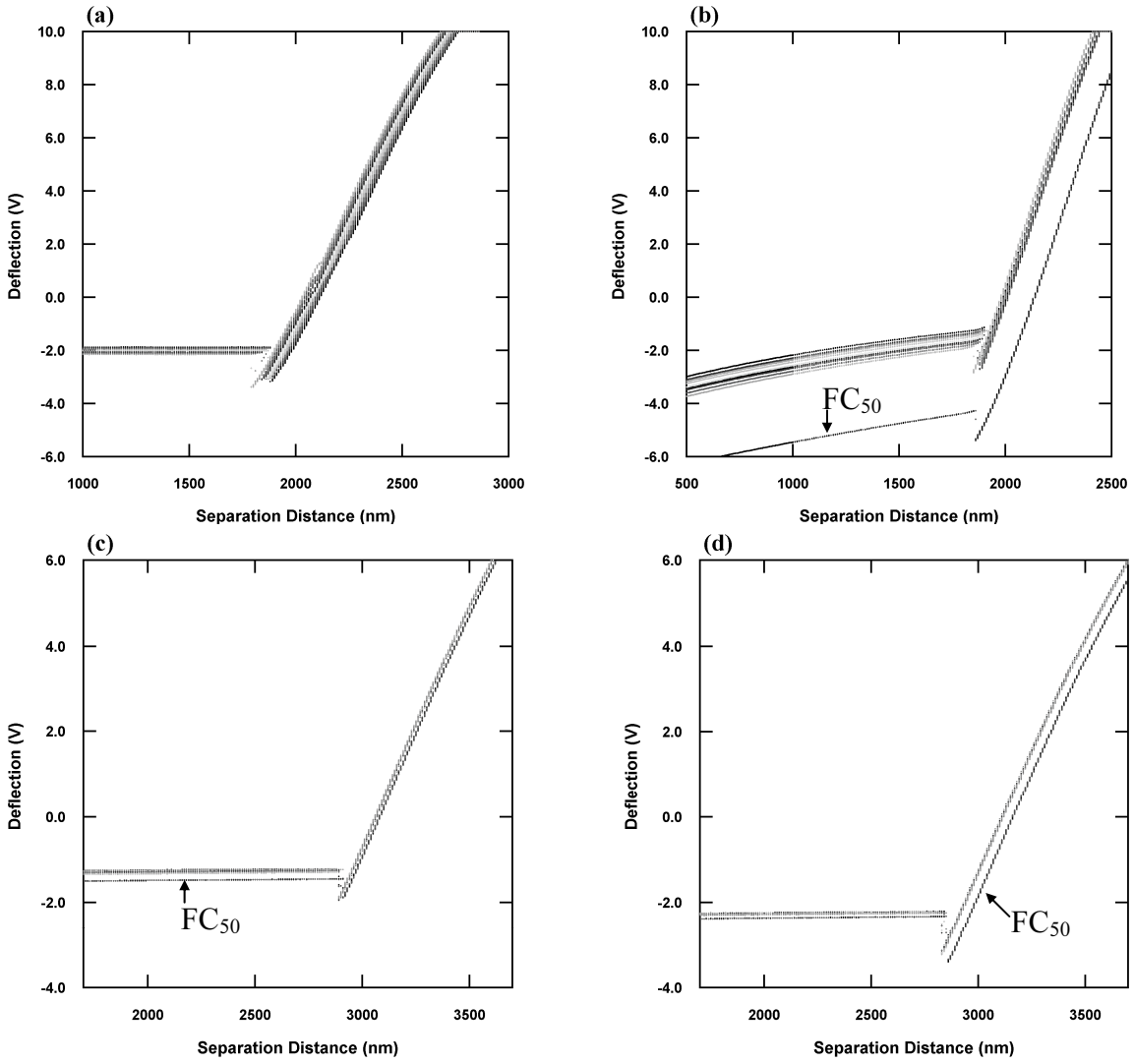

Figure 8: Deflection (V) as a function of separation distance (nm) for a 2 μm colloid approaching a polished quartz surface for system equilibration times of 0 (a), 20 (b), 30 (c) and 40 (d) minutes.

4.4. Preliminary Force Curves

To date, 90 series of measurements (30 to 100 force curves each) have been taken using the quartz surface, colloid-probes of varying characteristics (i.e., 1.0, 2.0 and 3.2 μm colloids, cantilevers of spring constants 0.055, 0.275, 0.305 N/m), and KCl solutions as described above. The majority of these measurements were made as an exercise to become familiar with 1) the AFM, 2) the colloid-probe technique, and 3) the complexities of the atmosphere in which the measurements were being made. Figure 9 shows typical data from the most recent measurements. These force curves were taken as a polished quartz surface approached a 2 μm colloid (k_s = 0.305 N/m) in KCl solutions of varying ionic strength at pH =6. It is clear that neither the relative trends between or absolute magnitudes of the force curves are reproducible. Because sufficient time was allowed for system equilibration, it is unlikely temperature effects are being observed. It is more likely that the discrepancies shown are a result of improper surface preparation

(i.e., one or both of the surfaces were dirty), or from impurities in the deionized water used. For all future measurements, greater atmospheric controls, including strict surface cleaning procedures, will be exercised, in addition to using high purity water (e.g., 18 MΩ) for all solutions. These methodological changes will lead to more accurate, precise AFM measurements. Because replicate direct force measurements have not yet been made, comparisons between direct observations (Figure 9) and theoretical predictions (Figure 6) are not possible.

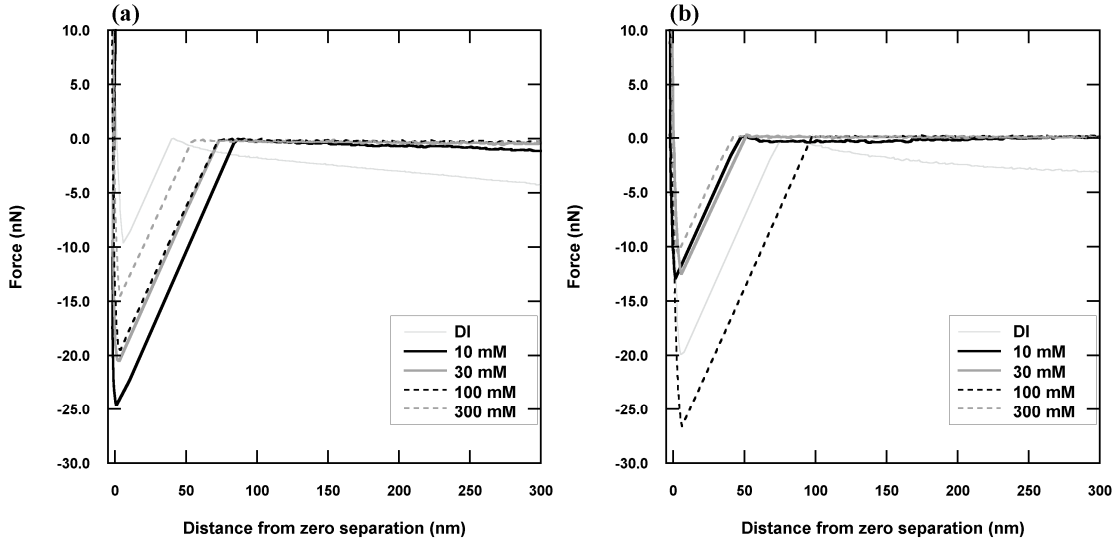

Figure 9: Replicate force (nN) versus distance from zero separation (nm) for a 2 μm colloid approaching a polished quartz surface in KCl solutions of varying ionic strength at pH =6.

5. Future Work

The work presented here provides a strong foundation for an investigation into the existence of a secondary energy minimum using direct force measurements obtained by Atomic Forces Microscopy. The immediate next step in this work is generating reproducible force measurements, which should be achievable through the use of more prudent cleaning procedures and high purity water for all electrolyte solutions. Once this step has been completed, a systematic set of force measurements will be made for all particle sizes with the quartz surface. This set of measurements will then be repeated for feldspar, biotite, and Plexiglas surfaces. Direct measurements will finally be compared to theoretical predictions (i.e., DLVO calculations made using electrokinetic properties for the exact system employed during force measurements). The completion of this research project is being undertaken as a Master's Thesis project for New Mexico Institute of Mining and Technologies' Hydrology Program.

6. References

Adamczyk, Z., J. Czarnecki, and P. Warszynski, Effect of fluctuations of the energy barrier on colloid stability, *J. Colloid Interface Sci.*, *106*, 299-306, 1985.

Adamson, A. W., and A. P. Gast, *Physical Chemistry of Surfaces*, John Wiley & Sons, Inc., New York, 1997.

Antelmi, D. A., and O. Spalla, Adsorption of Nanolatex Particles to Mineral Surfaces of Variable Surface Charge, *Langmuir*, *15*, 7478-7489, 1999.

Assemi, S., P. G. Hartley, P. J. Scales, and R. Beckett, Investigation of adsorbed humic substances using atomic force microscopy, *Colloids Surf. A*, *248*, 17-23, 2004.

Bales, R. C., C. P. Gerba, G. H. Grondin, and S. L. Jensen, Bacteriophage transport in sandy soil and fractured tuff, *Appl. Environ. Microbiol.*, *55(8)*, 2061-2067, 1989.

Biggs, S., J. L. Burns, Y. Yao-de, G. J. Jameson, and P. Jenkins, Molecular Weight Dependence of the Depletion Interaction between Silica Surfaces in Solutions of Sodium Poly(styrene sulfonate), *Langmuir*, *16*, 9242-9248, 2000.

Bolster, C. H., A. L. Mills, G. M. Hornberger, and J. S. Herman, Spatial distribution of deposited bacteria following miscible displacement experiments in intact cores, *Water Resour. Res.*, *35*, 1797-1807, 1999.

Bowen, W. R., and T. Doneva, Atomic Force Microscopy Studies of Membranes: Effect of Surface Roughness on Double-Layer Interactions and Particle Adhesion, *J. Colloid Interface Sci.*, *229*, 544-549, 2000.

Bowen, W. R., T. Doneva, and A. G. Stoton, The use of atomic force microscopy to quantify membrane surface electrical properties, *Colloids Surf. A*, *201*, 73-83, 2002.

Bowen, W. R., N. Hilal, R. W. Lovitt, and C. J. Wright, An atomic force microscopy study of the adhesion of a silica sphere to a silica surface--effects of surface cleaning, *Colloids Surf. A*, *157*, 117-125, 1999.

Bradford, S. A., J. Simunek, M. Bettahar, M. T. Van Genuchten, and S. R. Yates, Modeling Colloid Attachment, Straining, and Exclusion in Saturated Porous Media, *Environ. Sci. Technol.*, *37*, 2242-2250, 2003.

Bradford, S. A., S. R. Yates, M. Bettahar, and J. Simunek, Physical factors affecting the transport and fate of colloids in saturated porous media, *Water Resour. Res.*, *38*, **63**-61-**6**3-12, 2002.

Brant, J. A., and A. E. Childress, Membrane-Colloid Interactoins: Comparison of Extended DVLO Predictions with AFM Force Measurments, *Environ. Eng. Sci.*, *19*, 413-427, 2002.

Cooper, W. D., Coagulation of polydisperse colloidal systems, *Kolloid-Z*, *250*, 38-&, 1972.

Czarnecki, J., The effects of surface inhomogeneities on the interactions in colloidal systems and colloid stability, *Adv. Colloid Interfac.*, *24*, 283-319, 1986a.

Czarnecki, J., Effects of surface inhomogeneities on the interactions of colloidal systems and colloid stability, *Adv Colloid Interfac*, *24*, 283-319, 1986b.

Derjaguin, B. V., and L. Landau, *Acta Physichochim.*, *14*, 1941.

Ducker, W. A., T. J. Senden, and R. M. Pashley, Direct measurement of colloidal forces using an atomic force microscope, *Nature*, *353*, 239-241, 1991.

Ducker, W. A., T. J. Senden, and R. M. Pashley, Measurment of Fores in Liquids Using a Force Microscope, *Langmuir*, *8*, 1831-1836, 1992.

Dukhin, S. S., and J. Lyklema, Dynamics of colloidal particle interaction: incomplete desorption relaxation, *Faraday Discuss. Chem. Soc.*, *90*, 261-290, 1990.

Frens, G., On coagulation in the primary minimum, *Faraday Discuss. Chem. Soc.*, *65*, 146-155, 1978.

Frens, G., and J. T. G. Overbeek, Repeptization and the theory of electrocratic colloids, *J. Colloid Interface Sci.*, *38*, 376-387, 1972.

Gregory, J., Approximate Expressions for Retarded van der Waals Interaction, *J. Colloid Interface Sci.*, *83*, 138-145, 1981.

Grindrod, P., The impact of colloids on the migration and dispersal of radionuclides within fractured rock, *J. Contam. Hydrol.*, *13*, 167-191, 1993.

Grolimund, D., M. Elimelech, M. Borkovec, K. Barmettler, R. Kretzschmar, and H. Sticher, Transport of in Situ Mobilized Colloidal Particles in Packed Soil Columns, *Environ. Sci. Technol.*, *32*, 3562-3569, 1998.

Hahn, M. W., D. Abadzic, and C. R. O'Melia, Aquasols: On the Role of Secondary Minima, *Environ. Sci. Technol.*, *38*, 5915-5924, 2004.

Hahn, M. W., and C. R. O'Melia, Deposition and Reentrainment of Brownian Particles in Porous Media under Unfavorable Chemical Conditions: Some Concepts and Applications, *Environ. Sci. Technol.*, *38*, 210-220, 2004.

Hogg, R., T. W. Healy, and D. W. Fuerstenau, Mutual Coagulation of Colloidal Dispersions, *Trans. Faraday Soc.*, *66*, 1638-1651, 1965.

Israelachvili, J., *Intermolecular and Surface Forces*, Elsevier, London, 1992.

James, S. C., and C. V. Chrysikopoulos, Effective velocity and effective dispersion coefficient for finite-sized particles flowing in a uniform fracture, *J. Colloid Interface Sci.*, *263*, 288-295, 2003.

Keller, A. A., S. Sirivithayapakorn, and C. V. Chrysikopoulos, Early breakthrough of colloids and bacteriophage MS2 in a water-saturated sand column, *Water Resour. Res.*, *40*, 2004.

Kersting, A. B., D. W. Efurd, D. L. Finnegan, D. J. Rokop, D. K. Smith, and J. L. Thompson, Migration of plutonium in ground water at the Nevada Test Site, *Nature*, *397*, 56-59, 1999.

Kretzschmar, R., K. Barmettler, D. Grolimund, Y.-d. Yan, M. Borkovec, and H. Sticher, Experimental determination of colloid deposition rates and collision efficiencies in natural porous media, *Water Resour. Res.*, *33*, 1129-1137, 1997.

Li, X., T. D. Scheibe, and W. P. Johnson, Apparent Decreases in Colloid Deposition Rate Coefficients with Distance of Transport under Unfavorable Deposition Conditions: A General Phenomenon, *Environ. Sci. Technol.*, *38*, 5616-5625, 2004.

Lord, D. L. 2001. Atomic Force Microscopy Training Handouts. Petroleum Recovery Research Center, New Mexico Institute of Mining and Technology, Socorro, NM.

Lower, S. K., C. J. Tadanier, and M. F. Hochellla, Measuring interfacial and adhesion forces between bacteria and mineral surfaces with bilogical force microscopy, *Geochim. Cosmochim. Ac.*, *64*, 3133-3139, 2000.

Lyklema, J., *Fundamentals of Interface and Colloid Science*, Academic Press, London, 1991.

McCarthy, J. F., and J. M. Zachara, Subsurface transport of contaminants, *Environ. Sci. Technol.*, *23*, 495-502, 1989.

McKay, L. D., R. W. Gillham, and J. A. Cherry, Field experiments in fractured clay till: 2. Solute and colloid transport, *Water Resour. Res.*, *20*, 1149-1162, 1993.

Meinders, J. M., H. C. van der Mei, and H. J. Busscher, Depostion Efficiency and Reversibility of Bacterial Adhesion under Flow, *J. Colloid Interface Sci.*, *176*, 329-341, 1995.

Papadopoulos, K. D., and C.-C. Kuo, The van der Waals interaction between a colloid and its host pore, *Colloid. Surface.*, *46*, 115-125, 1990.

Prieve, D. C., and M. M. J. Lin, The effect of a distribution in surface properties on colloid stability, *J. Colloid Interface Sci.*, *86*, 17-25, 1982.

Redman, J. A., S. B. Grant, T. M. Olson, and M. K. Estes, Pathogen Filtration, Heterogeneity, and the Potable Reuse of Wastewater, *Environ. Sci. Technol.*, *35*, 1798-1805, 2001.

Redman, J. A., S. A. Walker, and M. Elimelech, Bacterial Adhesion and Transport in Porous Media: Role of the Secondary Energy Minimum, *Environ. Sci. Technol.*, *38*, 1777-1785, 2004.

Reimus, P. W. 1995. Transport of Synthetic Colloids through Single Saturated Fractures: A Literature Review. LA-12707-MS, Los Alamos National Laboratory, Los Alamos, N.M.

Roy, S. B., and D. A. Dzombak, Colloid release and transport processes in natural and model porous media, *Colloids Surf. A*, *107*, 245-262, 1996.

Saiers, J. E., G. M. Hornberger, and L. Liang, First- and seond-order kinetics approaches for modeling the transport of colloidal particles in porous media, *Water Resour. Res.*, *30*, 2499-2506, 1994.

Sengupta, A. K., and K. D. Papadopoulos, Electrical double-layer interaction between two eccentric spherical surfaces, *J. Colloid Interface Sci.*, *149*, 135-152, 1992a.

Sengupta, A. K., and K. D. Papadopoulos, van der Waals interaction between a colloid and the wall of its host spherical cavity, *J. Colloid Interface Sci.*, *152*, 534-542, 1992b.

Sirivithayapakorn, S., and A. Keller, Transport of colloids in saturated porous media: A pore scale observation of the size exclusion effect and colloidal acceleration, *Water Resour. Res.*, *39(4)*, 2003.

Smith III, F. G., and W. M. Deen, Electrostatic Double-Layer Interactions for Spherical Colloids in Cylindrical Pores, *J. Colloid Interface Sci.*, *78*, 444-465, 1980.

Smith III, F. G., and W. M. Deen, Electrostatic effects on the partitioning of spherical colloids between dilute bulk solution and cylindrical pores, *J. Colloid Interface Sci.*, *91*, 571-590, 1983.

Speilman, L. A., and S. K. Friedlander, Role of Electrical Double Layer in Particle Deposition by Convective Diffusion, *J. Colloid Interface Sci.*, *46*, 22-31, 1974.

Swanton, S. W., Modeling Colloid Transport in Groundwater; The Prediction of Colloid Stability and Retention Behaviour, *Adv. Colloid Interfac.*, *54*, 129-208, 1995.

Toikka, G., R. A. Hayes, and J. Ralston, Adhesion of Iron Oxide to Silica Studied by Atomic Force Microscopy, *J. Colloid Interface Sci.*, *180*, 329-338, 1996.

Tong, M., T. A. Camesano, and W. P. Johnson, Spatial Variation in Deposition Rate Coefficients of an Adhesion-Deficient Bacterial Strain in Quartz Sand, *Environ. Sci. Technol.*, *39*, 3679-3687, 2005.

Tufenkji, N., and M. Elimelech, Correlation Equation for Predicting Single-Collector Efficiency in Physicochemical Filtration in Saturated Porous Media, *Environ. Sci. Technol.*, *38*, 529-536, 2004a.

Tufenkji, N., and M. Elimelech, Deviation from the Classical Colloid Filtration Theory in the Presence of Repulsive DLVO Interactions, *Langmuir*, *20*, 10818-10828, 2004b.

Tufenkji, N., and M. Elimelech, Breakdown of Colloid Filtration Theory: Role of the Secondary Energy Minimum and Surface Charge Heterogeneities, *Langmuir*, *21*, 841-852, 2005.

Tufenkji, N., J. A. Redman, and M. Elimelech, Interpreting Deposition Patterns of Microbial Particles in Laboratory-Scale Column Experiments, *Environ. Sci. Technol.*, *37*, 616-623, 2003.

van Bree, J. L. M. J., J. A. Poulis, B. J. Verhaar, and K. Schram, The influence of surface irregularities upon the van der Waals forces between macroscopic bodies, *Physica*, *78*, 187-190, 1974.

van de Ven, T. G. M., On the role of ion size in coagulation, *J. Colloid Interface Sci.*, *124*, 138-145, 1988.

Verwey, E. K. W., and J. T. G. Overbeek, *Theory of Stability of Lyophobic Colloids*, Elsevier, Amsterdam, 1948.

Warszynski, P., and T. G. M. van de Ven, Electroviscous forces, *Faraday Discuss. Chem. Soc.*, *90*, 313-321, 1990.

Yao, K.-M., M. T. Habibian, and C. R. O'Melia, Water and Waste Water Filtration: Concepts and Applications, *Environ. Sci. Technol.*, *5*, 1105-1112, 1971.

Distribution

SANDIA INTERNAL (hard copy):

2	MS 0899	4536	Technical Library
2	MS 9018	8945-1	Central Technical Files
1	MS 0123	01011	LDRD Office (Donna L. Chavez)
1	MS0735	6115	Marissa D. Reno

SANDIA INTERNAL (electronic copy):

Ray E. Finley
Susan J. Altman
Martin Piech


Sandia National Laboratories